JACS
JOURNAL OF THE AMERICAN CHEMICAL SOCIETY
Communication
pubs.acs.org/JACS

Interfacial Energy Conversion in Ru^{II} Polypyridyl-Derivatized Oligoproline Assemblies on TiO_2

Da Ma,[†,§] Stephanie E. Bettis,[†,§] Kenneth Hanson,[†] Maria Minakova,[‡] Leila Alibabaei,[†] William Fondrie,[†] Derek M. Ryan,[†] Garegin A. Papoian,[‡] Thomas J. Meyer,[†] Marcey L. Waters,*[,†] and John M. Papanikolas*[,†]

[†]Department of Chemistry, CB 3290, University of North Carolina, Chapel Hill, North Carolina 27599, United States
[‡]Department of Chemistry and Biochemistry, University of Maryland, College Park, Maryland 20742, United States

Supporting Information

ABSTRACT: Solid-phase peptide synthesis has been applied to the preparation of phosphonate-derivatized oligoproline assemblies containing two different Ru^{II} polypyridyl chromophores coupled via "click" chemistry. In water or methanol the assembly adopts the polyproline II (PPII) helical structure, which brings the chromophores into close contact. Excitation of the assembly on ZrO_2 at the outer Ru^{II} in 0.1 M $HClO_4$ at 25 °C is followed by rapid, efficient intra-assembly energy transfer to the inner Ru^{II} (k_{EnT} = 3.0 × 10^7 s^{-1}, implying 96% relative efficiency). The comparable energy transfer rate constants in solution and on nanocrystalline ZrO_2 suggest that the PPII structure is retained when bound to ZrO_2. On nanocrystalline films of TiO_2, excitation at the inner Ru^{II} is followed by rapid, efficient injection into TiO_2. Excitation of the outer Ru^{II} is followed by rapid intra-assembly energy transfer and then by electron injection. The oligoproline/click chemistry approach holds great promise for the preparation of interfacial assemblies for energy conversion based on a family of assemblies having controlled compositions and distances between key functional groups.

Molecular structure and organization are key elements in molecular-level energy conversion. An object lesson is photosystem II in natural photosynthesis where light-driven oxidation of water occurs. Absorption of light in an antenna complex drives a sequence of five electron transfer reactions resulting in oxidative activation of the oxygen evolving complex and delivery of a reductive equivalent, as the semiquinone form of plastoquinone, separated by a distance of ~50 Å.[1,2]

At the heart of PSII is a structurally controlled array of light absorbers, electron transfer relays, and catalysts in the thylakoid membranes of chloroplasts. Mimicking these features, both in content and relative orientation, in an artificial device poses a significant synthetic challenge. We report here a systematic strategy based on solid-phase peptide synthesis (SPPS) combined with the copper catalyzed azide–alkyne cycloaddition (CuAAC or 'click' reaction) for modular synthesis of a spatially preorganized bichromophoric assembly.[3] This strategy has been applied to the preparation of an interfacial assembly for photochemical electron and energy transfer when bound in nanocrystalline films of TiO_2.

A number of strategies have been explored for the preparation of light harvesting assemblies including porphyrin arrays,[4] polymers,[5] DNA,[6] dendrimers,[7] metal–organic frameworks,[8] and molecular assemblies.[9] For interfacial applications, as in dye-sensitized solar cells (DSSC)[10] or dye-sensitized photoelectrosynthesis cells,[11] it is important to combine broad visible to near IR absorption with directional control of energy and electron transfer toward the semiconductor interface. Several examples of surface-bound assemblies have been discussed in the context of DSSCs[12] but lack detailed kinetic analysis of the excited-state photophysics.

Controlling the direction of electron and energy transfer requires the control of chromophore positioning and orientation relative to the surface as well as the ability to incorporate different chromophores at specific positions. Peptides are useful as molecular scaffolds for multiple functional units due to the ability to encode highly ordered secondary and tertiary structures based on their amino acid sequence. Oligoprolines with at least five proline residues are particularly notable in this regard because they form left-handed polyproline II (PPII) helices in polar solvents, providing a rigid scaffold for positioning multiple chromophores.[13] Additionally, SPPS allows for absolute control of the positioning of functional groups. With application of 'click' coupling, the amino acid sequence can be modified systematically with assembly structures by incorporating the appropriate functional groups (i.e., azide or alkyne) at specific locations in the peptide sequence.[3] This offers the additional advantage of incorporating molecular components with different functionalities (e.g., light-harvesting chromophores and molecular catalysts for water splitting) with a high degree of structural control.

The well-defined structural characteristics of oligoprolines[14] and other peptide scaffolds[15] have been exploited previously to investigate the distance dependence of electron and energy transfer in Ru^{II}-bpy modified derivatives. Herein, we report the design and synthesis of an oligoproline assembly containing two different chromophores on the surface of nanostructured films of TiO_2 and application of ultrafast transient spectro-

Received: January 7, 2013
Published: March 20, 2013

   dx.doi.org/10.1021/ja312143h | J. Am. Chem. Soc. 2013, 135, 5250–5253

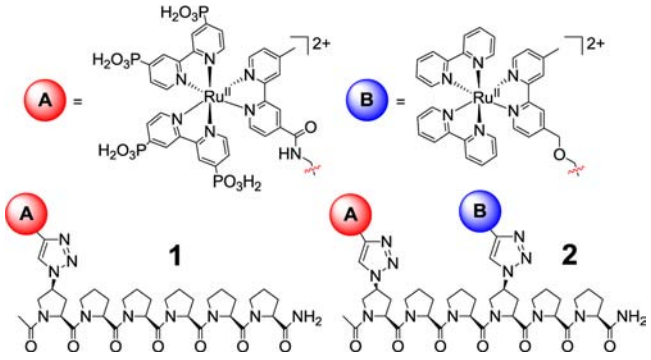

Figure 1. Structure of **1** and **2**.

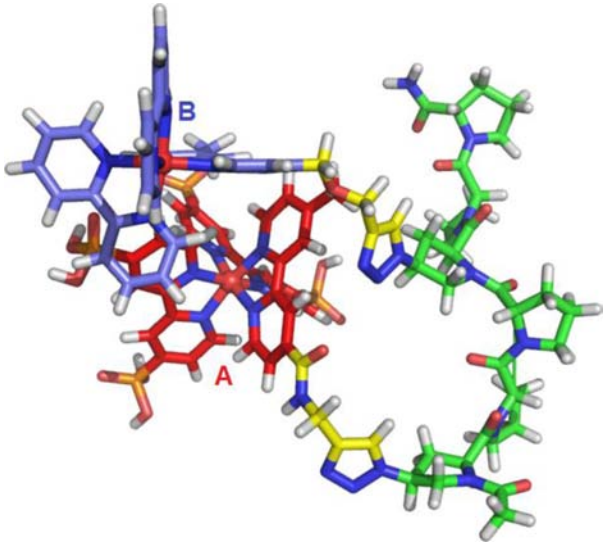

Figure 2. All-atom molecular dynamics simulation of **2** in solution showing the Ru^{II} chromophores in close contact. Green indicates oligoproline backbone, yellow indicates linkers, red indicates chromophore **A**, and blue indicates chromophore **B**.

scopic measurements to demonstrate and evaluate intra-assembly energy transfer and excited-state injection.

Two peptide-chromophore assemblies were investigated: Assembly **1** is a control compound containing only the inner chromophore **A**, which will bind directly to the surface, whereas assembly **2** contains both an inner and outer chromophore, **A** and **B**, respectively (Figure 1). The design of structure **2** was guided by: (1) having six proline residues to induce helical secondary structure; (2) including a Ru^{II} polypyridyl complex with phosphonate-derivatized bipyridine ligands for binding to metal oxide surfaces;[16] (3) using a two-proline spacer unit between the Ru^{II} chromophores, which in the PPII helix (Figure 2), aligns the two chromophores on the same side of the helix and minimizes their internuclear separation distance; (4) incorporating Ru^{II} chromophores with MLCT excited states "tuned" to create an energy transfer gradient toward the interface. Although subtle, the latter feature is present in **2** because of the electronic effects of the substituents on the π^* acceptor levels in the MLCT excited states of **A**. The unfunctionalized bpy ligands in **B** form an excited state that is slightly higher in energy than the functionalized ligands on **A**.

Assembly **1** was synthesized via SPPS with 4*S*-azido-L-proline coupled at the N-terminal position, followed by capping, cleavage from the resin, and subsequent solution-phase CuAAC to attach **A**. For **2**, the peptide was synthesized via SPPS up to the interior azidoproline at position 4, followed by on-bead CuAAC to attach **B**. SPPS was then continued to complete the peptide with azidoproline at the N-terminus and **A** was attached as for **1**. In this way, two different chromophores were attached in a position-dependent manner using the same coupling reaction without the use of orthogonal protecting group chemistry.

In water, at pH = 1.0, 4.0, and 7.4 or in MeOH, **2** exhibits left-handed PPII helical structure as indicated by circular dichroism (Figure S1). Molecular dynamics simulations support the formation of a PPII helical conformation (Figure 2) with the chromophores in close contact and an average Ru–Ru spacing of 13 Å (see SI).

The assemblies were loaded onto 3 μm thick, nanocrystalline (20 nm particles) films of TiO_2 or ZrO_2 by soaking the films overnight in a 150 μM solution of the peptide in aqueous 0.1 M $HClO_4$. Surface coverage was estimated by UV–visible measurements (Figure S6). Relative to $[Ru^{II}(bpy)_2(4,4'\text{-}(PO_3H_2)_2(bpy))]^{2+}$ (**RuP**), which exhibits full surface coverage[17] with $\Gamma = 8.6 \times 10^{-8}$ mol/cm^2 (2.9×10^{-8} mol/cm^2/μm), assemblies **1** and **2** have nearly full surface coverage with $\Gamma = 7.9 \times 10^{-8}$ mol/cm^2 and 7.1×10^{-8} mol/cm^2, respectively.

The dynamic events anticipated to occur following transient excitation of **2** on TiO_2 are illustrated in Scheme 1. Photon

Scheme 1. Schematic Representation of Photophysical Events of 2 on Nanocrystalline TiO_2

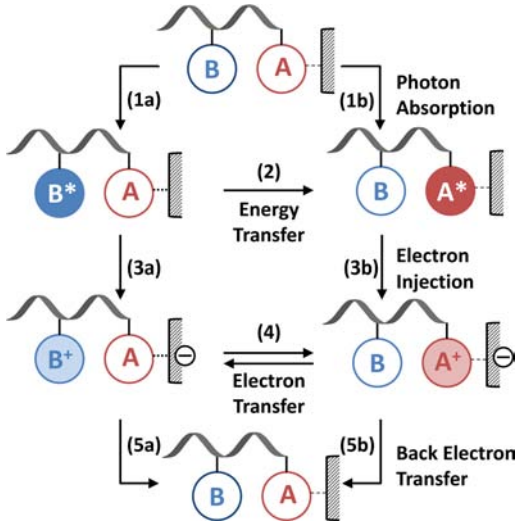

absorption can occur at either **A** or **B**. Photoexcitation at the **A** is expected to result in rapid electron injection into TiO_2 as observed for **RuP** on TiO_2 (Scheme 1, eq 1b).[17] Deactivation of **B*** can occur either by energy transfer to **A** (eq 2) followed by electron injection from **A*** (eq 3b) or by remote injection from **B*** (eq 3a). Following electron injection, electron transfer from **B** to A^+ (eq 4) is energetically favorable by ~130 mV as indicated by electrochemical measurements. Ultimately the electron in TiO_2 will recombine with the oxidized complex (A^+ or B^+) through back electron transfer (eq 5).

The energy transfer dynamics of **2** (Scheme 1, eq 2) were investigated by time-resolved emission measurements in aqueous 0.1 M $HClO_4$ at rt on the nanosecond time scale both in solution and on nanocrystalline ZrO_2 (where electron injection does not occur). As shown in Figure S7, excitation of

dx.doi.org/10.1021/ja312143h | J. Am. Chem. Soc. 2013, 135, 5250–5253

2 in solution and on ZrO_2 at 450 nm results in ^{3}MLCT emission with a time-dependent shift in the emission maximum from 630 to 645 nm. These observations are consistent with excitation of **B** (eq 1a) followed by intra-assembly energy transfer to **A**, (eq 2), which is favored by 70 meV (Figure S5). Analysis of the time-dependent emission data by application of model free global analysis resulted in τ_{EnT} = 31 ns in solution and τ_{EnT} = 33 ns on ZrO_2 (Figures S8–9 and Tables S1–2). The comparable energy transfer rate constants in solution and on nanocrystalline ZrO_2 suggest that the secondary structure of the oligoproline assembly is retained on the surface of ZrO_2.

Electron injection kinetics from **1*** and **2*** into nanocrystalline TiO_2 were measured by transient absorption spectroscopy (Supporting Information). In transient absorption difference spectra, obtained 600 fs after excitation at 475 nm, Figure 3,

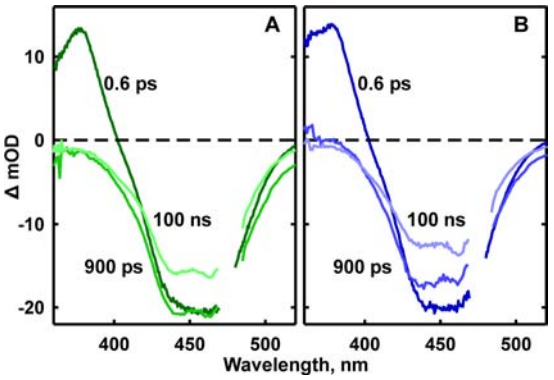

Figure 3. Transient absorption spectra of (a) **1** and (b) **2** at 0.6 ps (dark line), 900 ps (medium line), and 100 ns (light line) after laser excitation. Both samples were on 3 μm thick nanocrystalline TiO_2 film in aqueous 0.1 M $HClO_4$ at 25 °C. The excitation wavelength was 475 nm.

characteristic $\pi\pi^*$ absorptions appear at 375 nm for the reduced polypyridyl ligand radical anion characteristic of the MLCT excited state, along with a prominent ground-state bleach of ^{1}MLCT absorption band of **A** and **B** at 450 nm. For **1** and **2** the transient absorption feature at 375 nm disappears rapidly (<1 ns) leaving behind the 450 nm bleach. These spectral changes are a clear signature of electron injection from the assembly into TiO_2. On longer time scales, 100s of ns, the bleach recovers, due to recombination by back electron transfer of the injected electron in TiO_2 with the oxidized chromophore on the surface.

The intensity of the transient absorption signal at 375 nm is shown as a function of pump–probe delay in Figure 4. For both **1** and **2** an initial decay in the absorbance occurs in the first 20 ps (Figure 4a), indicative of rapid electron injection by **1*** and by inner chromophore **A*** in **2** (eqs 1b and 3b in Scheme 1). There is a presumably sub-100 fs injection component that lies within the instrument response and is not detected here, but has been reported for similar systems.[18] The initial decay is followed by a slower decay which becomes a bleach feature on the 100 ps to 1 ns time scale.[19] Kinetic analysis of the time-dependent absorbance changes for **1** and **2** over this time range (Figure 4a) were fit to biexponential kinetics with τ_1 = 20 and τ_2 = 200 ps (Table S3) with the difference being in the amplitudes. We estimate an injection efficiency for assembly **1** to be 56% based on the amplitude of the 405 nm transient absorption at 1 ns (SI).[17]

After 1 ns (Figure 4b), **1** decays by complex nonexponential kinetics over a period of several microseconds as found for **RuP** on TiO_2.[17] This is consistent with slow back electron transfer process (eq 5). Assembly **2**, on the other hand, shows a continued decrease in the amplitude of the excited-state absorption band over the next 100 ns, followed by a slow decay back to zero. Kinetic analysis of the data by multiexponential fit resulted in τ = 20 ns for the growth of a negative signal (Table S4).

The continued loss of excited-state absorption in **2** is indicative of delayed injection into TiO_2 that occurs with a 20 ns time constant. We attribute this delayed injection to excitation of the outer chromophore **B**, which then either injects remotely (eq 3a), or undergoes energy transfer to **A** (eq 2) followed by fast electron injection (eq 3b). Given the similarity in time scale for loss of excited-state absorption in **2** (20 ns) and intra-assembly energy transfer on ZrO_2 (~30 ns), we ascribe the delayed injection to the latter. In either case, these results point to high efficiency, ~96%, energy transfer/electron injection based on the relative lifetimes for excited-state decay (τ ~ 490 ns) and energy transfer/injection, and imply an injection efficiency for **2** of 54%. Therefore, **2** is an efficient antenna for interfacial sensitization by energy transfer.

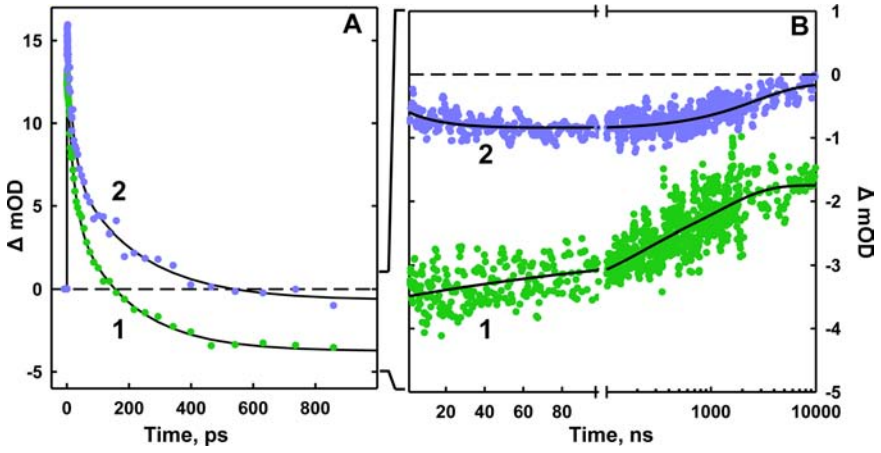

Figure 4. Transient absorption kinetics and fits of the $\pi\pi^*$ absorption (375 nm ±3 nm) for **1** (green) and **2** (blue) in a) the first 1000 ps and b) 1 to 10,000 ns after excitation at 475 nm. All samples were on 3 μm thick nanocrystalline TiO_2 film in aqueous 0.1 M $HClO_4$ solution at 25 °C.

dx.doi.org/10.1021/ja312143h | J. Am. Chem. Soc. 2013, 135, 5250–5253

The rates of back electron transfer are reflected in the decay of the ground-state bleach transient absorption signal at 450 nm (Figure S10). The back electron transfer kinetics for **1** and **2** exhibit multiexponential behavior due to the variety of back electron migration pathways in TiO_2, as shown previously for **RuP** under the same conditions.[17] The average lifetimes for recovery of the bleach at 450 nm, $<\tau>$, are 19 and 11 μs for assemblies **1** and **2**, respectively, compared to 17 μs for **RuP** (Table S5).[17] While the average back electron transfer time exceeds a microsecond, there is 20 ns component resulting presumably from direct excitation of **A** (eq 1b) that occurs along with the slower injection arising from excitation of **B** (Table S5). This 20 ns back electron transfer component makes it problematic to draw quantitative conclusions regarding injection efficiencies from the amplitudes of the kinetic components.

Our results are notable in introducing a new, modular approach to the synthesis of preorganized and highly tunable assemblies for interfacial molecular energy conversion using solid-phase peptide synthesis coupled with 'click' chemistry. We have demonstrated that such scaffolds maintain their secondary structure in solution and on surfaces as well as provide the necessary arrangement of chromophores for directional energy transfer followed by electron injection into TiO_2. We are currently synthesizing a family of multichromophoric oligoprolines to explore the distance dependence of intra-assembly electron and energy transfer. Additionally chromophore-catalyst assemblies are being investigated for applications in dye-sensitized photoelectrosynthesis cells.

■ ASSOCIATED CONTENT

Ⓢ Supporting Information

Experimental, theoretical methods, and data analysis. This material is available free of charge via the Internet at http://pubs.acs.org.

■ AUTHOR INFORMATION

Corresponding Author

mlwaters@email.unc.edu; john_papanikolas@unc.edu

Author Contributions

[§]These authors contributed equally.

Notes

The authors declare no competing financial interest.

■ ACKNOWLEDGMENTS

This material is based upon work wholly supported as part of the UNC EFRC Center for Solar Fuels, an Energy Frontier Research Center funded by the U.S. Department of Energy, Office of Science, Office of Basic Energy Sciences under award no. DE-SC0001011. We acknowledge the UNC SERC Instrumentation Facility funded by the U.S. Department of Energy, Office of Energy Efficiency and Renewable Energy, award no. DE-EE0003188.

■ REFERENCES

(1) Ferreira, K. N.; Iverson, T. M.; Maghlaoui, K.; Barber, J.; Iwata, S. *Science* **2004**, *303*, 1831.

(2) Gagliardi, C. J.; Vannucci, A. K.; Concepcion, J. J.; Chen, Z.; Amadelli, T. J. *Energy Environ. Sci.* **2012**, *5*, 7704.

(3) Kümin, M.; Sonntag, L.-S.; Wennemers, H. *J. Am. Chem. Soc.* **2007**, *129*, 466.

(4) Mozer, A. J.; Griffith, M. J.; Tsekouras, G.; Wagner, P.; Wallace, G. G.; Mori, S.; Sunahara, K.; Miyashita, M.; Earles, J. C.; Gordon, K. C.; Du, L.; Katoh, R.; Furube, A.; Officer, D. L. *J. Am. Chem. Soc.* **2009**, *131*, 15621. Uetomo, A.; Kozaki, M.; Suzuki, S.; Yamanaka, K.; Ito, O.; Okada, K. *J. Am. Chem. Soc.* **2011**, *133*, 13276.

(5) Fang, Z.; Eshbaugh, A. A.; Schanze, K. S. *J. Am. Chem. Soc.* **2011**, *133*, 3063. Liu, Y.; Summers, M. A.; Edder, C.; Fréchet, J. M. J.; McGehee, M. D. *Adv. Mater.* **2005**, *17*, 2960. Kim, Y.-G.; Walker, J.; Samuelson, L. A.; Kumar, J. *Nano Lett.* **2003**, *3*, 523. Wang, L.; Puodziukynaite, E.; Vary, R. P.; Grumstrup, E. M.; Walczak, R. M.; Zolotarskaya, O. Y.; Schanze, K. S.; Reynolds, J. R.; Papanikolas, J. M. *J. Phys. Chem. Lett.* **2012**, *3*, 2453.

(6) Dutta, P. K.; Varghese, R.; Nangreave, J.; Lin, S.; Yan, H.; Liu, Y. *J. Am. Chem. Soc.* **2011**, *133*, 11985. Garo, F.; Häner, R. *Angew. Chem., Int. Ed.* **2012**, *51*, 916.

(7) Gilat, S. L.; Adronov, A.; Fréchet, J. M. J. *Angew. Chem., Int. Ed.* **1999**, *38*, 1422. Hasobe, T.; Kashiwagi, Y.; Absalom, M. A.; Sly, J.; Hosomizu, K.; Crossley, M. J.; Imahori, H.; Kamat, P. V.; Fukuzumi, S. *Adv. Mater.* **2004**, *16*, 975.

(8) Lee, C. Y.; Farha, O. K.; Hong, B. J.; Sarjeant, A. A.; Nguyen, S. T.; Hupp, J. T. *J. Am. Chem. Soc.* **2011**, *133*, 15858. Kent, C. A.; Liu, D.; Ma, L.; Papanikolas, J. M.; Meyer, T. J.; Lin, W. *J. Am. Chem. Soc.* **2011**, *133*, 12940.

(9) Hu, K.; Robson, K. C. D.; Johansson, P. G.; Berlinguette, C. P.; Meyer, G. J. *J. Am. Chem. Soc.* **2012**, *134*, 8352. Huang, Z.; Geletii, Y. V.; Musaev, D. G.; Hill, C. L.; Lian, T. *Ind. Eng. Chem. Res.* **2012**, *51*, 11850.

(10) O'Regan, B.; Grätzel, M. *Nature* **1991**, *353*, 737.

(11) Song, W.; Chen, Z.; Brennaman, M. K.; Concepcion, J. J.; Patrocinio, A. O. T.; Murakami Iha, N. Y.; Meyer, T. J. *Pure Appl. Chem.* **2011**, *83*, 749.

(12) O'Regan, B.; Gratzel, M. *Nature* **1991**, *353*, 737. Amadelli, R.; Argazzi, R.; Bignozzi, C. A.; Scandola, F. *J. Am. Chem. Soc.* **1990**, *112*, 7099. Parussulo, A. L. A.; Iglesias, B. A.; Toma, H. E.; Araki, K. *Chem Commun.* **2012**, *48*, 6939. Kleverlaan, C.; Alebbi, M.; Argazzi, R.; Bignozzi, C. A.; Hasselmann, G. M.; Meyer, G. J. *Inorg. Chem.* **2000**, *39*, 1342.

(13) Deber, C. M.; Bovey, F. A.; Carver, J. P.; Blout, E. R. *J. Am. Chem. Soc.* **1970**, *92*, 6191.

(14) Serron, S. A.; Aldridge, W. S; Fleming, C. N.; Danell, R. M.; Baik, M.-H.; Sykora, M.; Dattelbaum, D. M.; Meyer, T. J. *J. Am. Chem. Soc.* **2004**, *126*, 14506. Striplin, D. R.; Reece, S. Y.; McCafferty, D. G.; Wall, C. G.; Friesen, D. A.; Erickson, B. W.; Meyer, T. J. *J. Am. Chem. Soc.* **2004**, *126*, 5282.

(15) Springer, J. W.; Parkes-Loach, P. S.; Reddy, K. R.; Krayer, M.; Jiao, J.; Lee, G. M.; Niedzwiedzki, D. M.; Harris, M. A.; Kirmaier, C.; Bocian, D. F.; Lindsey, J. S.; Holten, D.; Loach, P. A. *J. Am. Chem. Soc.* **2012**, *134*, 4589. Channon, K. J.; Devlin, G. L.; MacPhee, C. E. *J. Am. Chem. Soc.* **2009**, *131*, 12520. Hong, J.; Kharenko, O. A.; Ogawa, M. Y. *Inorg. Chem.* **2006**, *45*, 9974. Knorr, A.; Galoppini, E.; Fox, M. A. *J. Phys. Org. Chem.* **1997**, *10*, 484. Wilger, D. J.; Bettis, S. E.; Materese, C. K.; Minakova, M.; Papoian, G. A.; Papanikolas, J. M.; Waters, M. L. *Inorg. Chem.* **2012**, *51*, 11324. Hanson, K.; Wilger, D.; Jones, S. T.; Harrision, D. P.; Bettis, S. E.; Luo, H.; Papanikolas, J. M.; Waters, M. L.; Meyer, T. J. *Biopolymers* **2013**, *100*, 25.

(16) Hanson, K.; Brennaman, M. K.; Luo, H.; Glasson, C. R. K.; Concepcion, J. J.; Song, W.; Meyer, T. J. *ACS Appl. Mater. Interfaces* **2012**, *4*, 1462.

(17) Hanson, K.; Brennaman, M. K.; Ito, A.; Luo, H.; Song, W.; Parker, K. A.; Ghosh, R.; Norris, M. R.; Glasson, C. R. K.; Concepcion, J. J.; Lopez, R.; Meyer, T. J. *J. Phys. Chem. C.* **2012**, *116*, 14837.

(18) Asbury, J. B.; Ellingson, R. J.; Ghosh, H. N.; Ferrere, S.; Nozik, A. J.; Lian, T. *J. Phys. Chem. B* **1999**, *103*, 3110.

(19) Although dominated by the excited-state absorption at early times, the transient absorption signal has contributions from positive going signal due to the appearance of excited-state absorption and a negative going signal due to loss of ground-state absorption, i.e., bleach. The approach to an overall negative signal at 375 nm reflects the presence of a small bleach contribution at this wavelength that becomes apparent as the excited-state absorption band disappears due to injection.